



Experimental Study of the Triaxial Strength Properties of Hollow Cylindrical Granite Specimens Under Coupled External and Internal Confining Stresses

Shaofeng Wang^{1,2} · Xibing Li¹ · Kun Du^{1,3,4} · Shanyong Wang² · Ming Tao¹

Received: 31 August 2017 / Accepted: 8 March 2018 / Published online: 14 March 2018
© Springer-Verlag GmbH Austria, part of Springer Nature 2018

Abstract

High geostresses and stress gradients are the predominant stress conditions in deep excavation-disturbed rock masses. The aim of this study is to determine the triaxial compressive strength properties of hollow cylindrical granite specimens under a radially non-uniform confining stress field with different radial stress gradients determined by coupled external and internal confining stresses. Triaxial compression testing of hollow cylindrical rock specimens was performed to investigate the influence of the radial stress gradient, external confining stress and specimen length-to-diameter (L/D) ratio on the triaxial compressive strength. The experimental results and regressed failure criteria indicate that the triaxial compressive strengths of the hollow cylindrical granite specimens increase with the external confining stresses, but decrease with an increase in the radial stress gradients. The calculated goodness of fit (R^2) and root-mean-squared error suggest that the nonlinear failure criterion based on the Hoek–Brown model is more accurate than the linear failure criterion based on the Mohr–Coulomb model for determining the influences of the external confining stress and radial stress gradient on the triaxial compressive strength. In addition, the triaxial compressive strength increases with a decreasing L/D ratio due to the strengthening end effect of the hollow cylindrical granite specimens and the change in the failure pattern of these specimens from shear to slabbing.

Keywords Hollow cylindrical granite · Radial stress gradient · Length-to-diameter ratio · Triaxial compressive strength · Failure criterion

1 Introduction

High in situ geostresses and excavation-induced stress gradients are the predominant stress conditions in the rock masses surrounding the deep underground engineering

projects. These conditions induce excavation damage zones (Martino and Chandler 2004) and are prone to triggering specific types of rock failure that are different than those in shallow rock masses, e.g., rock spalling (Read 2004; Cai and Kaiser 2014), rock bursting (Hua and You 2001; Hoek and Martin 2014; Du et al. 2016; Li et al. 2018), large squeezing deformation (Cantiene and Anagnostou 2009) and zonal disintegration (Shemyakin et al. 1986; Tao et al. 2013). These phenomena influence the stabilities of the rock masses surrounding underground excavations. Thus, safety issues induced by the responses to excavation unloading in these surrounding rock masses under high initial in situ stress states have been a prominent focus in mining, tunnelling and hydropower engineering (Li et al. 2014). In practice, deep rock is under high in situ stress. As a cavern or tunnel is excavated, the initial stress field is disturbed and redistributed, creating non-uniform stress field around the excavation boundary (Cao et al. 2016). For a circular excavation in a massive elastic rock, the non-uniform stress distribution was solved by Kirsch's stress solution for a plate with a

✉ Kun Du
dukuncsu@csu.edu.cn
Shaofeng Wang
wsfcumt@163.com

¹ School of Resources and Safety Engineering, Central South University, Changsha 410083, People's Republic of China
² ARC Centre of Excellence for Geotechnical Science and Engineering, The University of Newcastle, Callaghan, NSW 2308, Australia
³ State Key Laboratory for Geomechanics and Deep Underground Engineering, Beijing 100083, China
⁴ Advanced Research Center, Central South University, Changsha 410083, People's Republic of China

central hole (Brady and Brown 2006). The non-uniformity of a stress field can be quantitatively characterized by the stress gradient, which is determined by many practical factors: the initial in situ geostress, rock conditions, excavation characteristics and support performances. The rock strength reflects the support capacity and determines the reliability of the underground excavation engineering. Therefore, the study to investigate the surrounding rock strength and failure under a non-uniform confining stress field can provide the basis for not only fundamental studies, but also practical applications.

Laboratory testing of hollow cylindrical rock specimens is a widely used method to establish complicated stress conditions and investigate the associated deformation, strength and fracture characteristics. This testing method has at least two advantages over conventional solid cylinder tests. The first advantage is that hollow cylinder tests can perform physical simulations under a reduced scale of the stress condition and stress path around the excavation boundary of deep caverns or tunnels (Hoskins 1969; Lee et al. 1999; Yang 2016). The second advantage is that tests using hollow cylindrical specimen can be used as an alternative true triaxial testing approach (Alsayed 2002; Dinis da Gama 2012).

Handin et al. (1967) suggested that ductility can be described as a linear function of the relative magnitude of the intermediate principal stress by subjecting hollow cylinders to combined triaxial compression or extension and torsion tests. Hoskins (1969) performed a series of experiments on thick-walled hollow cylindrical rock specimens under combined polyaxial stress conditions applied by internal, confining and axial loads; from these experiments, it was concluded that the magnitude of the intermediate principal stress, the presence of the compressive stress gradients, or both had a considerable and systematic effect on the rock strength. Lee et al. (1999) investigated the potential effect of the stress paths on the mechanical behaviour of sandstone using a series of hollow cylindrical triaxial tests, in which axial loading, outer and inner confining pressures, and torque were applied to the specimen. Alsayed (2002) utilized the Hoek triaxial cell and a specially designed internal pressure loading configuration for multiaxial testing of hollow cylinders; this configuration could apply uniaxial, biaxial, triaxial and polyaxial compression as well as indirect tension to evaluate rock behaviour, the results of which confirmed the influence of the intermediate principal stress and stress condition on the strength and failure of the rock. Zhang et al. (2011) carried out triaxial unloading experiments using thick-walled limestone cylindrical specimens to simulate the excavation unloading process by unloading the internal pressure to investigate rock splitting failure, which was then clarified by Han et al. (2016) on the basis of the Griffith strength theory. Li et al. (2015) investigated the

performance of support of the laneway or tunnel walls using conventional triaxial compression on thick-walled hollow sandstone cylinders by filling in the internal hole. Yang (2016) used a series of conventional triaxial compression tests to investigate the effect of the hole diameter on the deformation, strength and crack damage behaviour of hollow sandstone specimens under different confining pressures, the results of which indicated that the triaxial compressive strength of the hollow sandstone decreases linearly as the hole diameter increases. The work mentioned above has significantly contributed to the understanding of the influence of the stress condition and stress path on the mechanical behaviour of rock. Nevertheless, few experimental studies have focused on the quantitative effect of a non-uniform confining stress field with various stress gradients and there is little research on establishing a strength criterion model that includes coupled factors of confining stress and stress gradient.

Therefore, in this paper, a series of triaxial compression tests on thick-walled hollow cylindrical granite specimens were performed using the MTS-815 servo-controlled rock mechanics test system manufactured by MTS Systems Corporation in USA and a specially designed internal loading device. The experimental tests were conducted to determine the triaxial compressive strength properties of the rock under coupled external and internal confining stresses, which were scaled representations of the physical simulations of an in situ rock mass around a circular opening under a radial non-uniform confining stress condition. Based on the experimental results, the influences of the radial stress gradients, external confining stress magnitudes and specimen length-to-diameter (L/D) ratios on the triaxial compressive strengths and failure patterns of the hollow cylindrical granite specimens were analysed. Finally, the linear and nonlinear failure criteria of the hollow cylindrical granite specimens subjected to the coupled influences of an external confining stress and a radial stress gradient were established based on the Mohr–Coulomb criterion and empirical Hoek–Brown criterion, respectively.

2 Experiment Methodology

2.1 Preparation of the Rock Specimen

The rock specimens shown in Fig. 1 were cored from a large intact granite block. First, columnar specimens with a diameter of 50 mm and L/D ratios of 2, 1 and 0.5 were created. The top and bottom ends of the specimens were polished to ensure that the two surfaces were smooth and parallel. Subsequently, a cylindrical hole with a diameter of 6 mm was drilled through the centre of the specimen. This type of specimen is called a thick-walled hollow cylindrical rock.

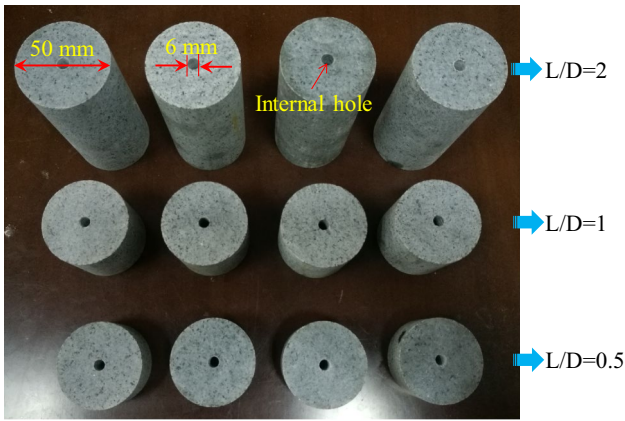


Fig. 1 Hollow cylindrical granite specimens used in the present study

All the experiments were performed on dry rock specimens at room temperature. The average P-wave velocity of the tested granite is 5351 m/s. The average density of the tested granite specimens is 2.765 g cm⁻³.

2.2 Test Apparatus

All the experiments were performed in a MTS-815 servo-controlled rock mechanics test system, as shown in Fig. 2. The system consists of five main units: the axial loading unit (Fig. 2a), external oil pressure loading unit (Fig. 2a, c), internal water pressure loading unit (Fig. 2a, b), displacement- and stress-monitoring unit (Fig. 2a), and computerized data acquisition and control unit (Fig. 2d). The system uses a coupled loading function to apply an axial force, external oil pressure and internal water pressure to the rock specimen. The maximum loading capacities of the axial force, external oil pressure and internal water pressure are 2600 kN, 140 MPa and 140 MPa, respectively. During the test, the axial deformation was measured by a pair of linear variable displacement transducers (LVDTs).

During the loading process of the internal confining stress, the water, which is a pressure-transmitting medium, may seep into the rock specimen and induce uncertain effects on the mechanical properties of the tested rock specimen.

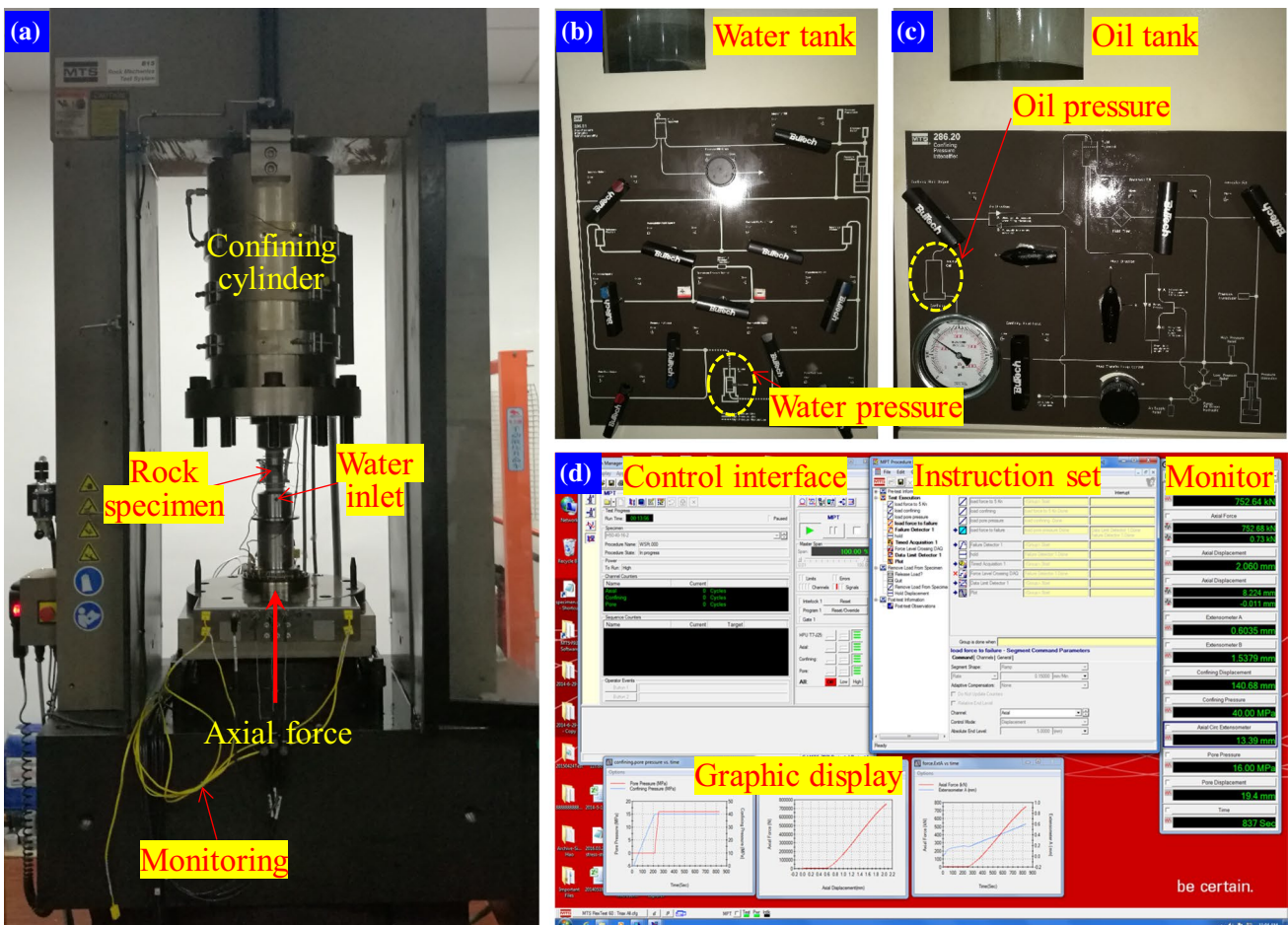


Fig. 2 Photographs of the test system that includes a a conventional triaxial loading frame, b an internal water pressure loading system, c an external oil pressure loading system and d control software

To avoid the problem mentioned above, an internal loading device, shown in Fig. 3, was designed to apply the water pressure to the internal boundary face of the rock specimen. The cross-sectional view (Fig. 3a) and the images of the assembled loading device (Fig. 3b) show the assembly of the internal loading device and hollow cylindrical specimen. The photograph in Fig. 3c shows that the internal loading device consists of six parts: the upper cover, lower cover, waterproof hose, pressed seal cone, fixing bolt and threaded hole. The water supplied from the internal water pressure loading unit was sealed in the internal loading device by the waterproof hose and pressed seal cone. The waterproof hose isolated the water from the rock specimen and external oil pressure loading unit, thereby preventing water from penetrating the rock, influencing the rock strength and permeating into the oil-filled confining cylinder. The waterproof hose is a soft and flexible pipe that can expand freely to

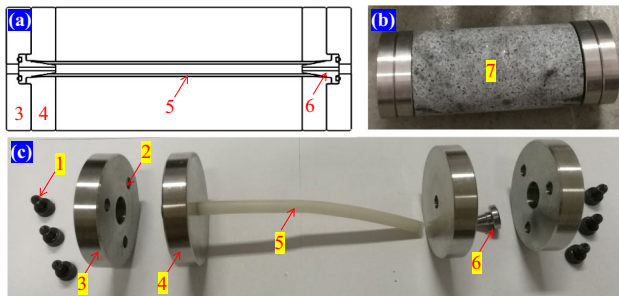
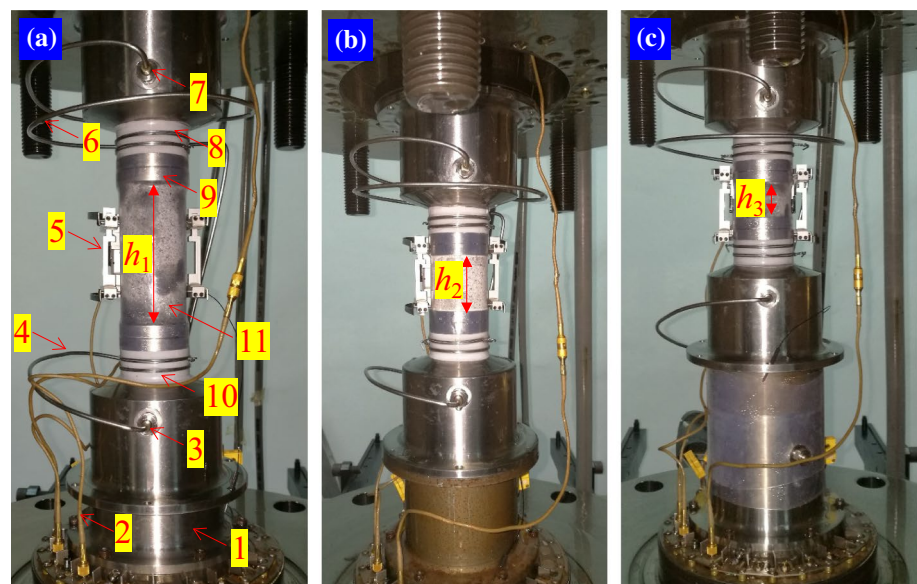


Fig. 3 Loading device for applying the water pressure to the internal boundary face of the hollow cylindrical granite: **a** the cross-sectional profile, **b** the assembled diagram with a rock specimen, and **c** the disassembled diagram of the parts. 1—Fixing bolt; 2—Threaded hole; 3—Upper cover; 4—Lower cover; 5—Waterproof hose; 6—Pressed seal cone; 7—Hollow cylindrical granite specimen

Fig. 4 Loading combinations designed for the tests of the hollow cylindrical specimens with L/D ratios of **a** 2, **b** 1 and **c** 0.5. 1—Base; 2—Data transmission line; 3—Lower water inlet; 4—Lower water pipe; 5—Axial LVDT; 6—Upper water pipe; 7—Upper water inlet; 8—Tightened wire; 9—Internal loading device; 10—Seal tape; 11—Heat-shrinkable tube; h_1 , h_2 and h_3 —Rock specimens with the lengths of 100, 50 and 25 mm, respectively



contact the internal boundary face of the hollow cylindrical rock; when this occurs, the internal water pressure can be completely transmitted and applied to the internal boundary face. The upper cover, seal cone and lower cover were pressed by the axial force to achieve a satisfactory seal and transmitted the axial force to the end faces of the rock specimen.

2.3 Testing Procedure

In the tests, the coupled external and internal confining stresses were applied to the external and internal boundary faces of a hollow cylindrical specimen using the oil pressure loading unit and water pressure loading unit, respectively. The axial stress was applied to the end faces of the specimen using the axial loading unit. The tests were carried out under different combinations of external and internal confining stresses. There were four applied external confining stresses: 10, 20, 40 and 60 MPa. The six internal confining stresses were 0, 20, 40, 60, 80 and 100% of each external confining stress magnitude. The test procedure performed to apply these stresses consisted of the following three steps:

1. The loading combinations shown in Fig. 4 were assembled and placed on the base. The setup includes a data transmission line, water pipes and inlets, internal loading device, hollow cylindrical granite specimen with different L/D ratios of 2 (Fig. 4a), 1 (Fig. 4b) or 0.5 (Fig. 4c), and axial LVDTs. The heat-shrinkable tube, sealing tapes and tightened wires were used to seal the specimen and prevent hydraulic oil from penetrating the rock.
2. Then, the external and internal confining stresses were successively increased to the designed levels at a con-

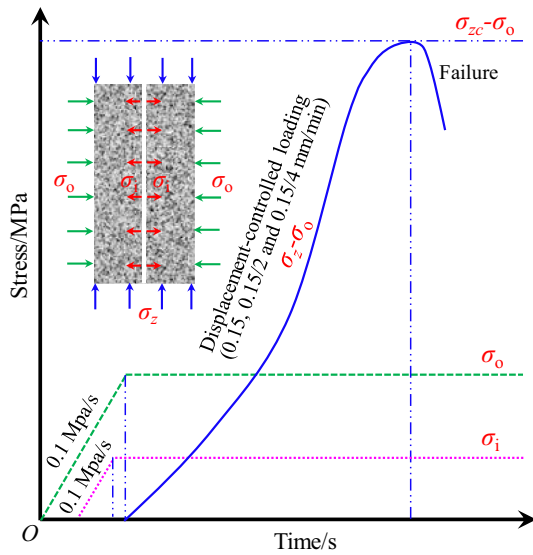


Fig. 5 Loading paths and stress combinations for the tests, where σ_o is the external confining stress, σ_i is the internal confining stress, σ_z is the axial stress, $\sigma_z - \sigma_o$ is the deviatoric axial stress, and σ_{zc} is the triaxial compressive strength of the rock specimen

stant rate of 0.1 MPa/s using the loading paths plotted in Fig. 5. The external confining stress was supplied by the oil-filled confining cylinder in which the rock specimen was submerged. The internal confining stress was provided by the water-filled waterproof hose placed through the cylindrical hole in the centre of the rock specimen.

- Next, a deviatoric axial stress was applied to the top face of the specimen by a rigid loading bar using a displacement-controlled loading approach, as shown in Fig. 5. The loading paths had an approximately constant strain rate of $2.5 \times 10^{-5} \text{ s}^{-1}$. Correspondingly, the loading velocities should be set to 0.15, 0.075 or 0.0375 mm/min, respectively, corresponding to the three L/D ratios of the specimens. Using the above loading paths, each rock specimen was compressed until failure, in accordance with the method suggested by the International Society for Rock Mechanics (ISRM) (Fairhurst and Hudson 1999).

2.4 Stress Analysis

During testing of a hollow cylindrical granite specimen, a thick-walled ring is subjected to coupled external and internal confining stresses on its outside and inside boundary faces in the radial–tangential plane, respectively. The stress analysis involves a thick-walled ring confined by uniform internal and external stresses, as shown in Fig. 6a. According to elastic theory under plane strain conditions (Sadd 2014), the plane stress field on the section perpendicular to the axial direction is expressed as

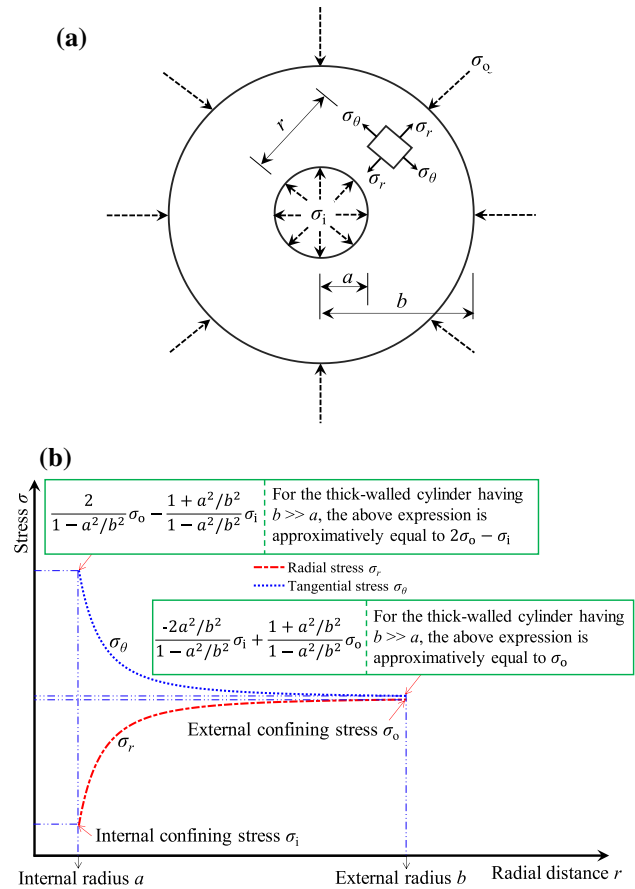


Fig. 6 Illustration of the plane stress analysis on the section perpendicular to the axial direction, which includes **a** a plane stress diagram and **b** curves of the change in the radial and tangential normal stresses along the radial direction

$$\sigma_r(r) = \frac{b^2/r^2 - 1}{b^2/a^2 - 1} \sigma_i + \frac{1 - a^2/r^2}{1 - a^2/b^2} \sigma_o \tag{1}$$

$$\sigma_\theta(r) = -\frac{b^2/r^2 + 1}{b^2/a^2 - 1} \sigma_i + \frac{1 + a^2/r^2}{1 - a^2/b^2} \sigma_o \tag{2}$$

$$\tau_{r\theta} = 0, \tag{3}$$

where σ_r is the radial normal stress, σ_θ is the tangential normal stress, $\tau_{r\theta}$ is the shear stress, σ_o is the external confining stress, σ_i is the internal confining stress, r is the radial distance from the centre, and a and b are the internal radius and external radius of the hollow cylindrical specimen.

The radial and tangential normal stress curves are plotted in Fig. 6b. The radial normal stress increases with distance from the internal boundary of the specimen along the radial direction. In contrast, the tangential normal stress decreases. However, the normal stresses are constant in the tangential direction. The plane stress field, for various external and internal confining stresses, is a non-uniform radial stress

field. The average radial stress gradient can reflect the overall rate of change and degree of non-uniformness of the stress distribution along the radial direction. The average radial stress gradients of the radial and tangential normal stresses are given by Eqs. (4) and (5), respectively.

$$\bar{\nabla}\sigma_r = \frac{\int_a^b \sigma'_r(r)dr}{b-a} = \frac{\sigma_o - \sigma_i}{b-a} \quad (4)$$

$$\bar{\nabla}\sigma_\theta = \frac{\int_a^b \sigma'_\theta(r)dr}{b-a} = \frac{\sigma_i - \sigma_o}{b-a}, \quad (5)$$

where $\bar{\nabla}\sigma_r$ and $\bar{\nabla}\sigma_\theta$ are the average radial stress gradients of the radial and tangential normal stresses, respectively. The gradients are either positive or negative, but have the same absolute value, indicating that the radial and tangential stress distributions have equal gradients along the radial direction from the internal to external boundary faces of the hollow cylindrical specimen.

3 Experimental Results

3.1 Stress–Strain Curve

The representative axial deviatoric stress–strain curves of the hollow cylindrical granite specimens recorded during the triaxial compression tests under the coupled external and internal confining stresses are illustrated in Fig. 7a–c, corresponding to the specimens with L/D ratios of 2, 1 and 0.5, respectively. The peak deviatoric stresses, which indicate the axial compressive capacities of the granite specimens, significantly increase with the external confining stresses and slightly increase with the internal confining stresses. The peak deviatoric stresses increase as the L/D ratios decrease under the same combination of external and internal confining stress conditions. Figure 7a illustrates that the granite specimen with the L/D ratio of 2 presents an elastic–brittle behaviour. Figure 7b, c shows that the deformation behaviour of the granite specimens with the L/D ratios of 1 and 0.5 varies from elastic–brittle to elastic–plastic properties as the confining stresses increase. There is a distinct elastic–plastic behaviour when the external and internal confining stresses are larger than 60 MPa and 40% of the external confining stress, respectively, for the granite specimens with the L/D ratio of 1. However, the granite specimens with the L/D ratio of 0.5 clearly present elastic–plastic behaviour when the external and internal confining stresses are greater than 40 MPa and 40% of the external confining stress, respectively. Under relatively low confining stresses, the deformation properties of the granite specimens with the L/D ratios of 1 and 0.5 do not present a uniform behaviour similar to

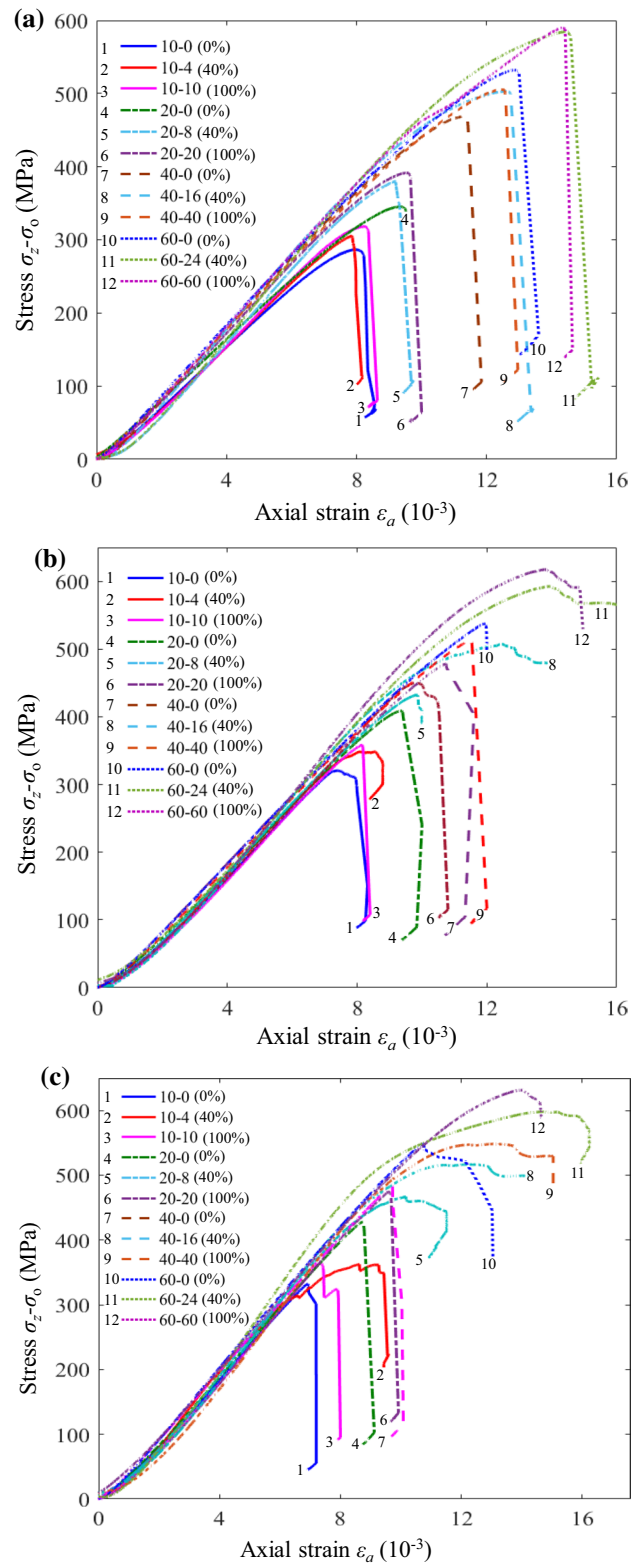


Fig. 7 Typical axial deviatoric stress–strain curves from the triaxial compression tests for hollow cylindrical granite specimens with the L/D ratios of **a** 2, **b** 1 and **c** 0.5 under coupled external and internal confining stresses, where the legend of the applied confining stresses are denoted in the following way: for example, for 10–4 (40%), the applied external confining stress is 10 MPa and the applied internal confining stress is 40% of the external confining stress, or 4 MPa

that of the specimens with the L/D ratio of 2. This phenomenon may result from the different failure patterns among specimens with varying L/D ratios and the differences in the mechanical properties of the specimens that are difficult to be weakened under lower confining stresses.

3.2 Triaxial Compressive Strength

The detailed triaxial compressive strength parameters of the hollow cylindrical granite specimens under the coupled external and internal confining stresses are listed in Table 1. The corresponding average radial stress gradients calculated by all the combinations of the external and internal confining stresses using Eq. (4) are also listed in Table 1. In Table 1, σ_{zc} represents the triaxial compressive strength of the granite specimen, which is obtained by adding the external confining stress to the corresponding axial peak deviatoric stress, and UCS represents the uniaxial compressive strength of the hollow cylindrical specimen. Three to five specimens were tested under each

combination of external and internal confining stresses. A dispersion coefficient, which was expressed by the ratio of the difference between the maximum and minimum values to the average value (Yang 2016), can be used to evaluate the discreteness of the tested granite specimens. The maximum dispersion coefficient is only 3.58%, which indicates that the difference in the triaxial compressive strengths between different specimens is very small under the same testing conditions. Therefore, the average strength values listed in Table 1 can be used to analyse the influences of the non-uniform stress parameters (external confining stress and average stress gradient) and specimen size (L/D ratio) on the triaxial compressive strength of the tested granite material under different non-uniform confining stress fields determined by the coupled external and internal confining stresses. Generally, the triaxial compressive strength increases with an increasing external confining stress and decreasing average radial stress gradient and L/D ratio. The detailed correlations are discussed in Discussion section.

Table 1 Loading conditions and experimental results

Confining pressure σ_o (MPa)	Internal pressure σ_i (MPa)	Average stress gradient $\bar{\nabla}\sigma_r$ (MPa/mm)	Average strength σ_{zc} (MPa)		
			Height 100 mm ($H/D=2$)	Height 50 mm ($H/D=1$)	Height 25 mm ($H/D=0.5$)
0 (UCS)	–	–	210.25	262.63	283.37
10	0	0.455	310.63	330.35	342.18
	2	0.364	315.08	339.45	350.22
	4	0.273	326.03	358.26	372.54
	6	0.182	326.17	361.14	373.41
	8	0.091	327.69	362.63	375.59
	10	0	328.02	368.05	374.43
20	0	0.909	365.21	428.56	448.09
	4	0.727	376.04	444.72	462.86
	8	0.545	400.16	452.01	487.36
	12	0.364	403.23	456.12	491.33
	16	0.182	408.49	469.01	493.21
	20	0	411.61	469.48	494.96
40	0	1.818	508.78	518.17	525.44
	8	1.455	516.90	526.76	540.69
	16	1.091	542.95	547.33	556.73
	24	0.727	543.12	547.55	583.26
	32	0.364	543.74	548.87	586.14
	40	0	545.31	551.62	588.31
60	0	2.727	592.22	596.94	608.09
	12	2.182	609.40	624.19	633.76
	24	1.636	645.08	652.36	658.22
	36	1.091	647.01	667.14	672.55
	48	0.545	647.93	671.53	687.53
	60	0	649.68	677.29	691.46

UCS uniaxial compressive strength

3.3 Failure Pattern

As shown in Fig. 8, the hollow cylindrical rocks with the same L/D ratio present similar failure patterns, even under different combinations of external and internal confining stresses. Thus, it was considered that the radial stress gradient has an inconspicuous influence on the failure pattern of the hollow cylindrical granite specimens. However, the failure pattern changes with the L/D ratios of the specimens. The typical failure of the specimens with different L/D ratios is shown in the photographs in Fig. 9. It is seen from the lateral views that shear failure dominates the failure pattern at $L/D=2$ (Fig. 9a). The top and bottom views show that a few small radial and tangential cracks occur on the end faces of the specimens. Figure 9c shows that the numerous fractures are approximately perpendicular to the end faces, as seen from the lateral wall of the specimen with $L/D=0.5$. A tangential annular crack and many radial cracks outside the ring occur on the end faces of the specimen with $L/D=0.5$. The failure pattern in this case is called slabbing failure (Li et al. 2011). The failure pattern of the specimen with $L/D=1$ might be coupled shear and slabbing, which is a transitional state from shear

failure to slabbing failure, as shown in Fig. 9b. At $L/D=1$, there is a mixture of shear and slabbing fractures on the lateral wall, and cracks formed by the connection of the radial and tangential cracks occur on the end faces of the specimen. When the L/D ratio increases from 0.5 to 2, the angle of the macro-fracture plane, which is defined as the angle between the normal to the fracture plane and the axial direction, decreases from approximately 90° to approximately 70° and the number of cracks significantly decreases. The increase in the triaxial compressive strengths of the specimens as their L/D ratios decrease may be caused by the end effect and the change in the failure patterns. Since the slabbing fractures are approximately parallel to the loading direction, the specimen will undergo a stage of plasticity and can withstand a further increase in the load, although numerous slabbing cracks have formed.

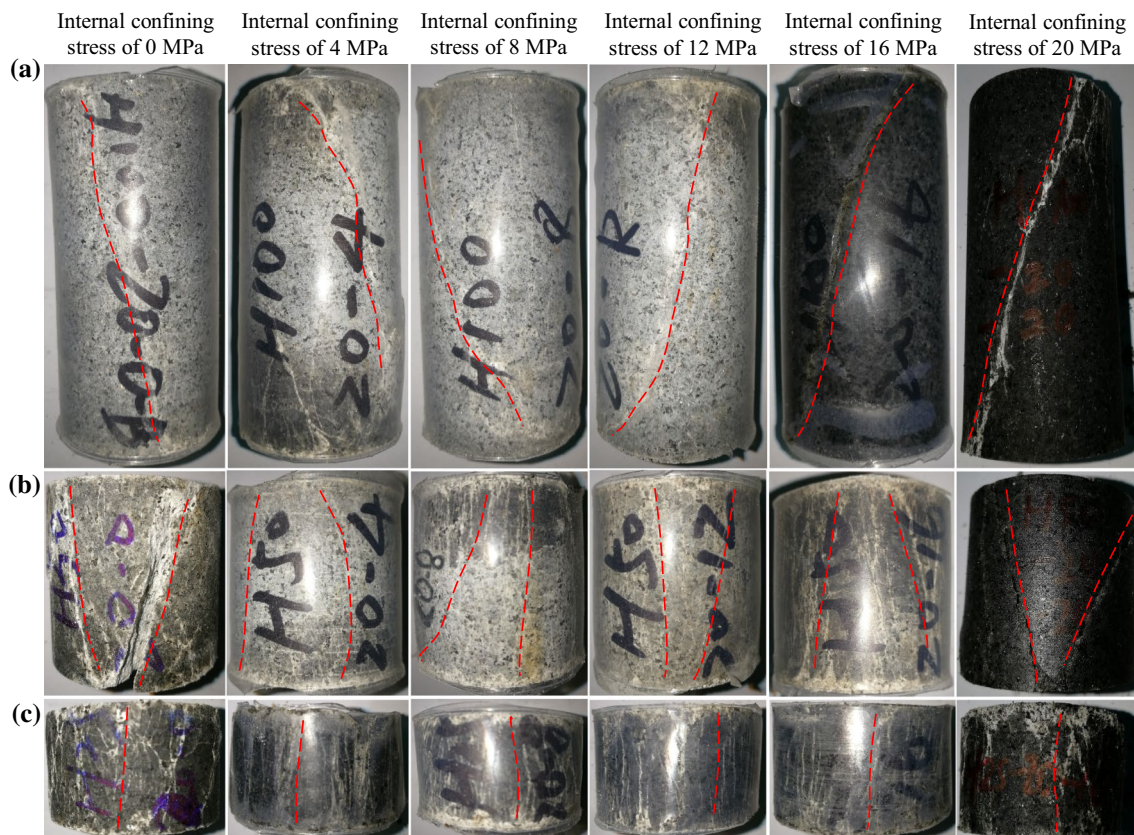


Fig. 8 Photographs of the failure, shot from the lateral faces of the hollow cylindrical granite specimens with the L/D ratios of **a** 2, **b** 1 and **c** 0.5 under different internal confining stresses at the same external confining stress of 20 MPa

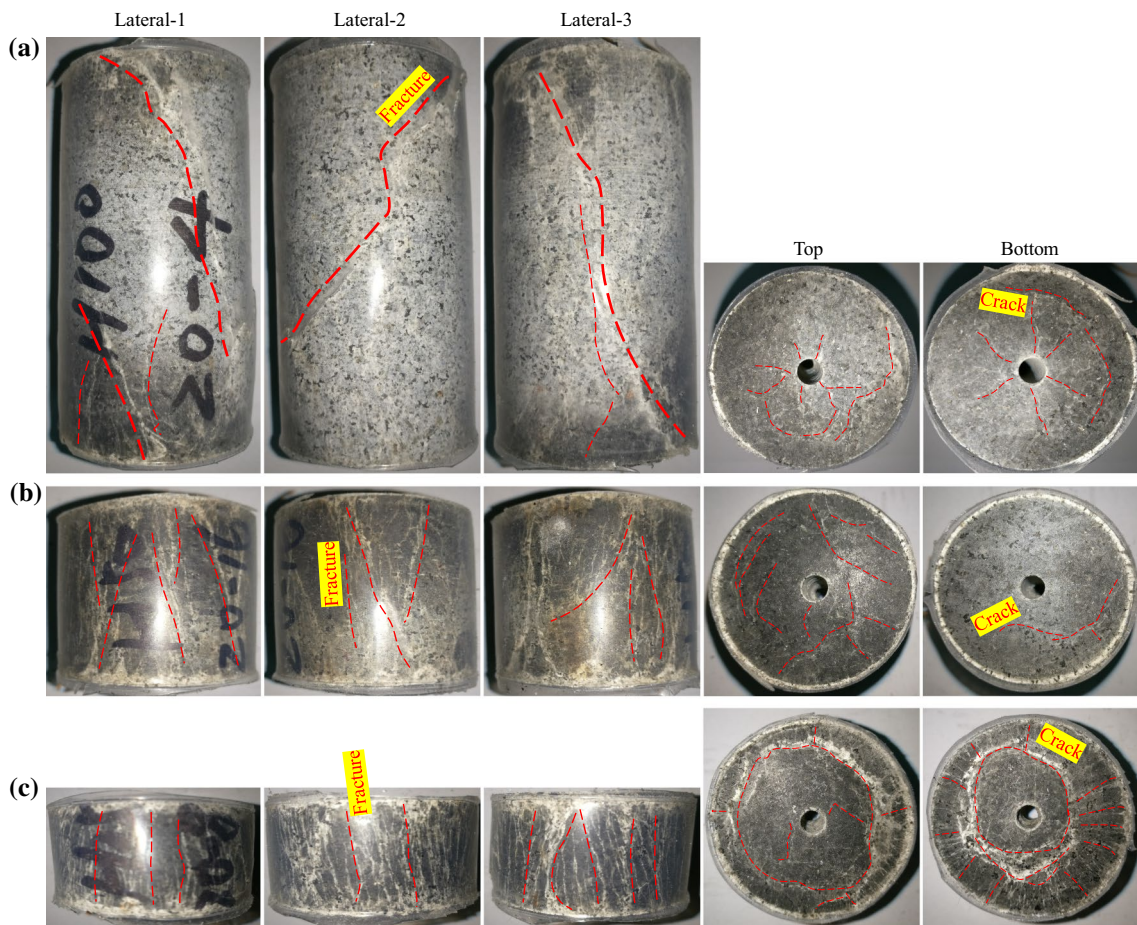


Fig. 9 Photographs of the typical failure, shot from the lateral, top and bottom faces of the hollow cylindrical granite specimens with the L/D ratios of **a** 2, **b** 1 and **c** 0.5

4 Discussion

4.1 Influence of the Radial Stress Gradient on the Strength

The triaxial compressive strengths of the hollow cylindrical granite specimens measured during the triaxial compression tests are plotted versus the average stress gradients and are shown in Fig. 10. The strengths are expressed as ranges and average values. The average stress gradients are determined by the different combinations of external and internal confining stresses according to Eq. (4). It is evident that the triaxial compressive strength presents a fast followed by slow nonlinear increase as the average stress gradient decreases at the same confining pressure and L/D ratio. This result indicates that the moderate confining stress applied to the internal boundary can clearly improve the triaxial bearing capacity of the hollow cylindrical granite specimens. In general, the rate of increase in the strength slows when the internal confining stress exceeds 40% of the external confining stress, providing an experimental validation that moderate support on the wall of the opening

can significantly improve the overall compressive strength of the rock mass around the opening when the opening is excavated along the direction of the maximum principal geostress.

The normalized indices of the triaxial compressive strength and average radial stress gradient were proposed to further analyse the influence of the radial stress gradient on the triaxial compressive strength of the hollow cylindrical granite specimens. These two normalized indices can be expressed as Eqs. (6) and (7), respectively.

$$\sigma_{zcn} = \frac{\sigma_{zc, \sigma_{oi}}}{\max(\sigma_{zc, \sigma_{oi}})} = \frac{\sigma_{zc, \sigma_{oi}}}{\sigma_{zc, \sigma_{oi}=\sigma_{ii}}} \quad (6)$$

$$\bar{\nabla}\sigma_m = \frac{\bar{\nabla}\sigma_{r, \sigma_{oi}}}{\max(\bar{\nabla}\sigma_{r, \sigma_{oi}})} = \frac{\bar{\nabla}\sigma_{r, \sigma_{oi}}}{\sigma_{oi}/(b-a)}, \quad (7)$$

where σ_{zcn} and $\bar{\nabla}\sigma_m$ are the normalized indices of the triaxial compressive strength and radial stress gradient, $\sigma_{zc, \sigma_{oi}}$ and $\bar{\nabla}\sigma_{r, \sigma_{oi}}$ are the measured strength and applied radial stress gradient in a triaxial compression test under the i th external

Fig. 10 Relation curves between the triaxial compressive strength and average stress gradient obtained from the tests under external confining stresses of 10, 20, 40 and 60 MPa (colour figure online)

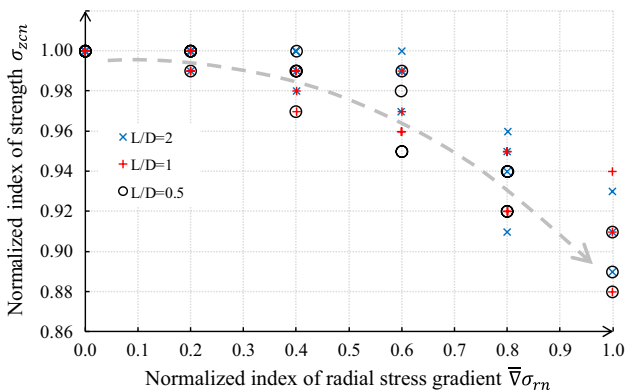
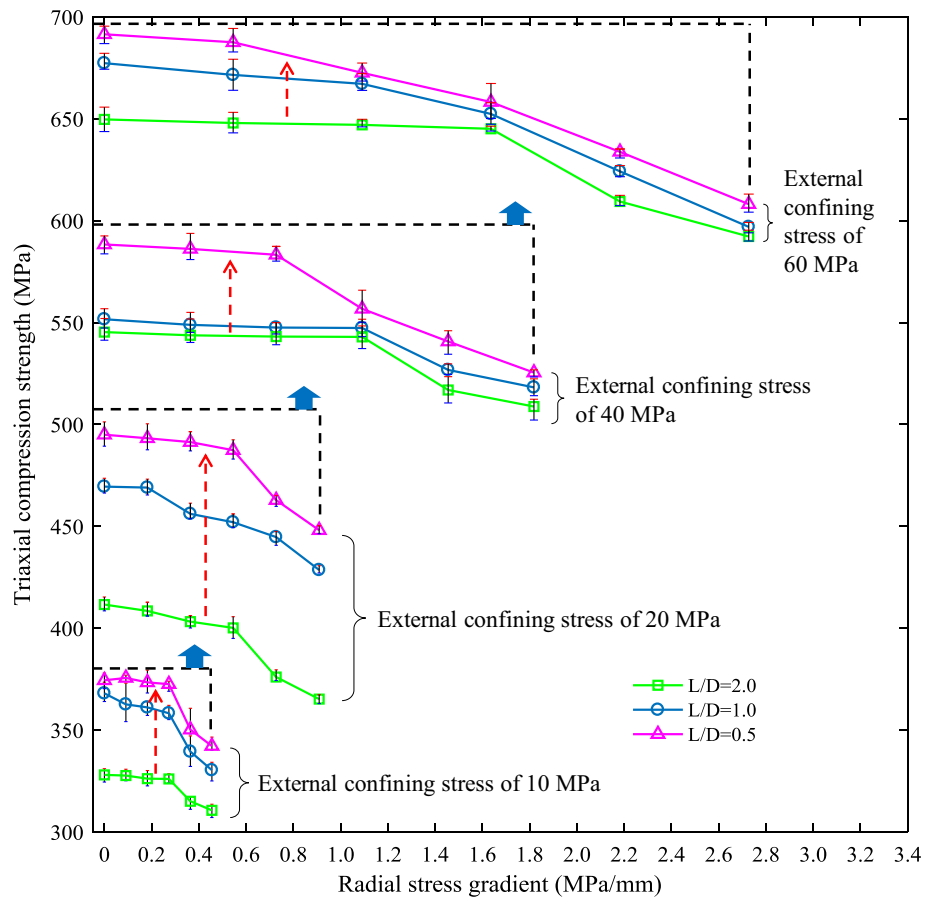


Fig. 11 Relation between the normalized indices of the triaxial compressive strength and radial stress gradient

confining stress level of σ_{oi} , and $\sigma_{zc, \sigma_{oi}=\sigma_{oi}}$ is the triaxial compressive strength when the applied external and internal confining stresses are equal under the i th external confining stress level of σ_{oi} .

The normalized indices were calculated and are plotted in Fig. 11, according to the data listed in Table 1 and Eqs. (6) and (7). Figure 11 shows that the normalized index

of the triaxial compressive strength decreases slowly and then quickly as the normalized index of radial stress gradient increases. That result supports the conclusion that the radial stress gradient has a negative influence on the triaxial compressive strength. In addition, the normalized indices of the strengths of the hollow cylindrical specimens with different L/D ratios have a similar decreasing trend with increasing normalized indices of the radial stress gradients.

The results can be explained as follows. When the internal confining stress does not equal the external confining stress, the radial and tangential normal stresses present a non-uniform distribution in the radial direction. A large stress gradient indicates high non-uniformity. A non-uniform stress distribution results in the retrogression of the triaxial compressive strength compared to that of the hollow cylindrical specimen under a uniform confining stress field when the internal and external confining stresses are equal. The negative influence of a non-uniform stress distribution on the strength of sandstone material with various hole diameters has been confirmed using conventional triaxial compression tests (Yang 2016). In fact, all the rock elements in a hollow cylindrical rock specimen are completely under true triaxial stress conditions, in which the confining stresses consist of radial and tangential normal stresses that are determined by

the different external and internal confining stresses applied to the outside and inside boundary faces. For a rock element, the high radial stress gradient reflects the large difference between the intermediate and minimum principal stresses when the hollow cylindrical specimen is under a certain external confining stress. Under a low radial stress gradient, the positive influence of the increasing intermediate principal stress and the negative influence of the decreasing minimum principal stress on the triaxial compressive strength can offset, resulting in only a small variation in the strength. Under a high radial stress gradient, however, the large difference between the intermediate and minimum principal stresses will cause a significant decrease in the triaxial compressive strength.

4.2 Influence of the External Confining Stress on the Strength

There are only six average radial stress gradients evaluated in the tests with a certain external confining stress. In addition, the applied average radial stress gradients vary among the different external confining stresses. Therefore, for an applied average radial stress gradient, there are only a few tests that can be used to evaluate the influence of the external confining stress on the triaxial compressive strength under a certain average radial stress gradient. Thus, a linear interpolation estimator expressed as Eq. (8) was proposed to

predict the strength values between the measured strengths to evaluate the influence of the external confining stress on the triaxial compressive strength of the specimens under more stress gradients.

$$\sigma_{zcj} = \frac{\sigma_{zc,i+1} - \sigma_{zc,i}}{\bar{\nabla}\sigma_{r,i+1} - \bar{\nabla}\sigma_{r,i}} (\bar{\nabla}\sigma_{r,j} - \bar{\nabla}\sigma_{r,i}) + \sigma_{zc,i}; \bar{\nabla}\sigma_{r,j} \in (\bar{\nabla}\sigma_{r,i}, \bar{\nabla}\sigma_{r,i+1}), \tag{8}$$

where $\bar{\nabla}\sigma_{r,i}$ and $\bar{\nabla}\sigma_{r,i+1}$ are the average radial stress gradients at the i th and $(i + 1)$ th measured levels under a certain external confining stress, respectively; $\sigma_{zc,i}$ and $\sigma_{zc,i+1}$ are the corresponding triaxial compressive strengths of the specimens, respectively; $\bar{\nabla}\sigma_{r,j}$ is the average radial stress gradient at the j th interpolated value between the i th and $(i + 1)$ th measured values; and $\sigma_{zc,j}$ is the corresponding triaxial compressive strength.

The relation curves between the external confining stresses and triaxial compressive strengths at the average stress gradients of 0.273, 0.455, 0.727, 0.909, 1.091 and 1.818 MPa/mm are shown in Fig. 12. The triaxial compressive strengths of the hollow cylindrical granites increase with increasing external confining stresses. This result is valid for all evaluated conditions of the average radial stress gradients, as shown by the blue arrows in Fig. 10, and is similar to the conventional triaxial compressive strength of intact cylindrical specimens, as expressed in both the classic Mohr–Coulomb criterion and the empirical Hoek–Brown

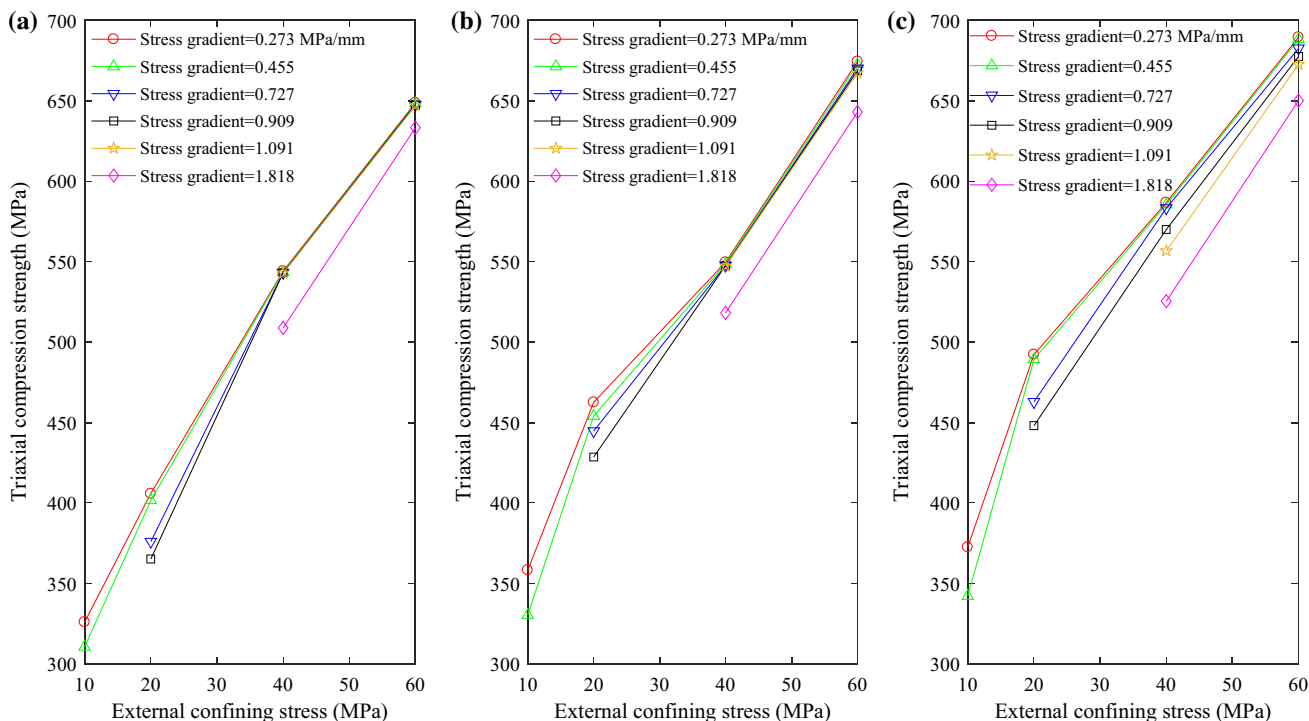


Fig. 12 Relation curves between the triaxial compressive strength and external confining stress obtained from the tests of the hollow cylindrical specimens with the L/D ratios of **a** 2, **b** 1 and **c** 0.5

criterion (Franklin 1971; Hoek and Brown 1980; Jaeger et al. 2007). In fact, an increase in the external confining stress under a certain radial stress gradient will cause increases in the intermediate and minimum principal stresses for each rock element in a hollow cylindrical specimen, resulting in the increase in its triaxial compressive strength. Further, the increased triaxial compressive strength of each rock element will increase the triaxial compressive strength of the entire rock specimen.

4.3 Influence of the L/D Ratio on the Strength

The relation curves between the triaxial compressive strengths and L/D ratios under the average stress gradients of 0.273 and 0.455 MPa/mm are plotted in Fig. 13 as examples of the influence of the specimen L/D ratio on its triaxial compressive strength. Figure 13 shows that the triaxial compressive strength of the specimens increases with a decreasing L/D ratio. This result is valid for all evaluated conditions of the average radial stress gradients, as shown by the red dotted arrows in Fig. 10, and may be caused by the end effect and the change in the failure pattern with L/D ratios. The end effect can apply a certain lateral confinement to the specimen, in which the relative scale of the confined zone formed by the end effect increases as the L/D ratio decreases and usually becomes more significant when the specimen is squatter ($L/D < 2$) (Bieniawski and Bernede 1979; Heuze 1980; Martin and Maybee 2000; Mogi 2007; Xu et al. 2017). In addition, supported by the external confining stress, the hollow cylindrical granite specimen with the low L/D ratio underwent a stage of plasticity and can

sustain further loading even though many slabbing cracks formed on the external wall.

4.4 Influence of the L/D Ratio on the Failure Pattern

It can be seen from Figs. 8 and 9 that the failure patterns change from shear failure to slabbing failure as the specimen L/D ratio decreases from 2 to 0.5. This result is due to the size and end effects in the triaxial compression tests, as illustrated in Fig. 14. For the size effect, the specimen with the L/D ratio of 1 is approximately equivalent to the combination of the top and bottom quarter sections of the specimen with the L/D ratio of 2. Similarly, the specimen with the L/D ratio of 0.5 can be seen as the combination of the top and bottom quarter sections of the specimen with the L/D ratio of 1. For the end effect, the end friction between the axial loading bar and specimen will produce a lateral confining stress, which increases as the L/D ratio decreases. The applied external and internal confining stresses in the tests cannot change the failure pattern. For the case when the external and internal confining stresses are equal, the test is equivalent to a conventional triaxial compression test for an intact cylindrical specimen. In that case, the fracture angle at rock failure is expressed as $\alpha = \pi/4 + \varphi/2$ according to the Mohr–Coulomb failure criterion (Brady and Brown 2006), where φ is the friction angle of the rock. At each confining stress, the increase in the measured triaxial compressive strength induced by the end effect will cause the friction angle measurements to increase, resulting in the increase in the fracture angle. Thus, the greater influence of the end effect will induce rotation of the fracture as the L/D ratio of the specimens decrease from 2 to 0.5, resulting in an

Fig. 13 Relation curves between the triaxial compressive strength and L/D ratio obtained from the tests under the average radial stress gradients of **a** 0.273 MPa/mm and **b** 0.455 MPa/mm

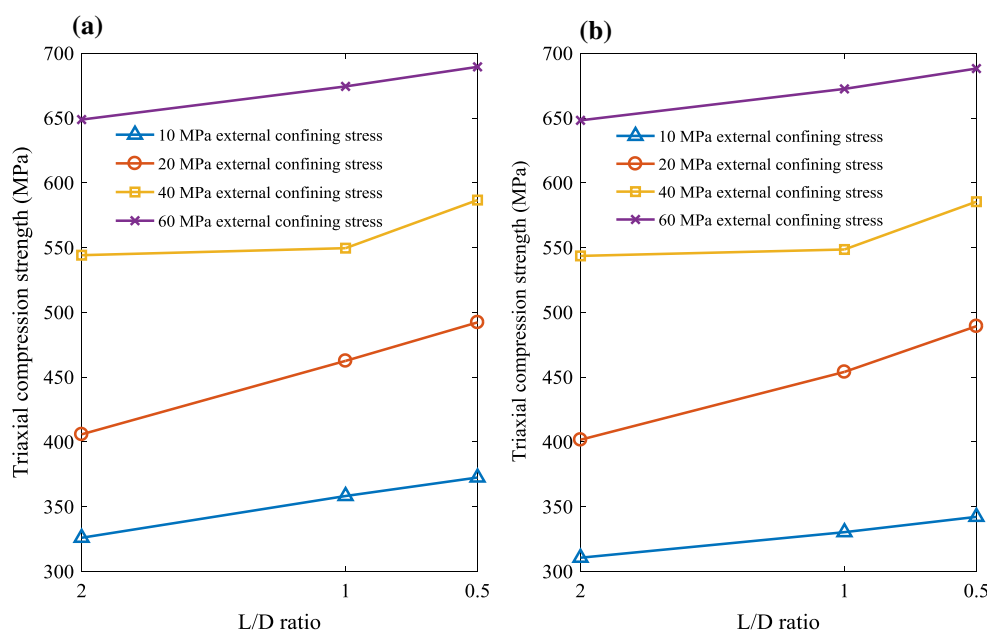
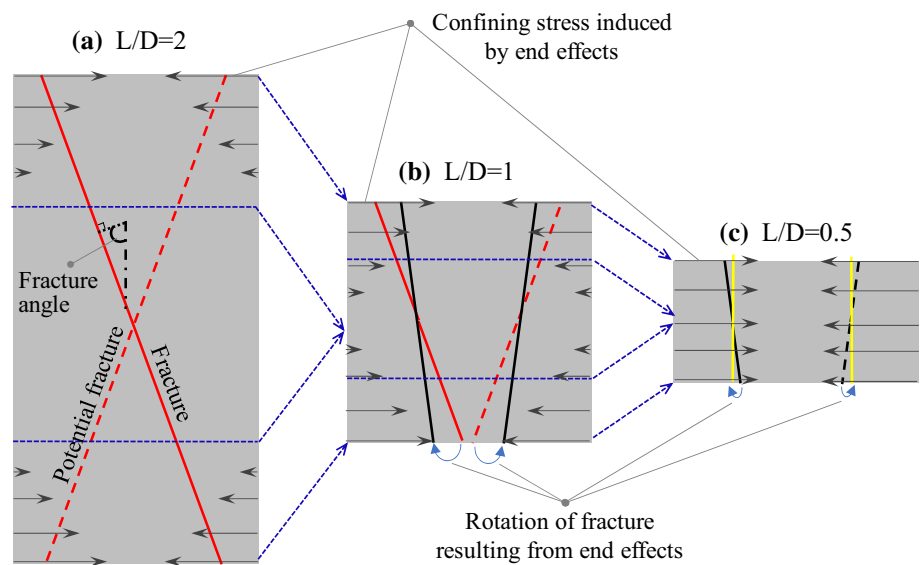


Fig. 14 Schematic diagrams of the failure patterns of the hollow cylindrical granite specimens with the L/D ratios of **a** 2, **b** 1 and **c** 0.5 and their transformation processes



increase in the fracture angle and a variation in the failure patterns, which change from shear failure to slabbing failure.

4.5 Failure Criterion

Failure criteria were used to determine the failure of rock under the different stress conditions, which were measured and regressed from conventional and true triaxial compression tests and tensile tests. Based on the experimental strength data, some valuable two-/three-dimensional failure criterion models were proposed, such as the Mohr–Coulomb criterion (Brady and Brown 2006), Hoek–Brown criterion (Hoek and Brown 1997), D–P criterion (Drucker and Prager 1952), Mogi criterion (Mogi 2007) and Wiebols–Cook criterion (Wiebols and Cook 1968). These failure criteria can be used to determine whether a rock element in a numerical or theoretical model of a rock mass undergoes failure and to analyse the stability of the rock mass. However, a rock mass is usually subjected to complex and non-uniform stress conditions, unlike the uniform stress conditions of a rock element, complicating the entire stability analysis of a rock mass structure. It is challenging for tunnelling and mining engineer to use complicated numerical and theoretical analyses. Therefore, a regressed failure criterion based on experimental strengths from physical simulations of rock mass structures is useful for stability analysis in tunnelling and mining engineering.

In this section, the Mohr–Coulomb (Brady and Brown 2006) and Hoek–Brown (Hoek and Brown 1997; Brady and Brown 2006) failure criteria are used to establish the linear and nonlinear failure criteria, respectively, to investigate the effects of the non-uniform confining stress distribution parameters, including the radial stress gradient and external confining stress, on the triaxial compressive strength of

the hollow cylindrical granite specimens. In this case, the triaxial compression experiment on the hollow cylindrical granite specimens under coupled external and internal confining stresses is a scaled physical simulation of the rock mass around a circular opening oriented along the direction of maximum principal geostress.

Based on the Mohr–Coulomb failure criterion in Eq. (9), the linear failure criterion determining the rock failure under a non-uniform confining stress field can be proposed and expressed as Eq. (10), assuming that the external confining stress and radial stress gradient have linear effects on the triaxial compressive strength of the hollow cylindrical granite specimens.

$$\sigma_s = \sigma_c + k\sigma_o \tag{9}$$

$$\sigma_s = \sigma_c + k\sigma_o + \mu_1 \frac{\sigma_o - \sigma_i}{b - a}, \tag{10}$$

where σ_s is the triaxial compressive strength of the hollow cylindrical rock, σ_c is the uniaxial compressive strength of the rock material, and k and μ_1 are the coefficients reflecting the influences of the external confining stress and average radial stress gradient on the triaxial compressive strength of rock, respectively.

The goodness of fit (R^2), which expresses the fitting degree of the regressed values relative to the experimental results, and the root-mean-squared error (RMSE), which is a frequently used error measurement tool based on the difference between the regressed and the experimental results, are used to estimate the output quality of the regressed failure criterion model. Based on the data listed in Table 1 and the linear criterion expressed in Eq. (10), the coupled influences of the external confining stress and radial stress gradient on the triaxial compressive strength of the hollow

cylindrical granite specimens can be quantified and are shown in Fig. 15a. For the granite specimens with different L/D ratios, the regressed strength parameters, R^2 values and RMSEs are listed in Table 2.

Based on the empirical Hoek–Brown failure criterion given by Eq. (11), the single nonlinear failure criterion can be written as Eq. (12), assuming that the external confining stress and radial stress gradient have nonlinear and linear effects on the triaxial compressive strength of the hollow cylindrical granite specimens, respectively. In addition, the double nonlinear failure criterion can be expressed as Eq. (13), assuming that the external confining stress and radial stress gradient have nonlinear effects on the triaxial compressive strength of the hollow cylindrical granite specimens.

$$\sigma_s = \sigma_o + (m\sigma_c\sigma_o + \sigma_c^2)^{0.5} \quad (11)$$

$$\sigma_s = \mu_2 \frac{\sigma_o - \sigma_i}{b - a} + \sigma_o + (m\sigma_c\sigma_o + \sigma_c^2)^{0.5} \quad (12)$$

$$\sigma_s = \mu_3 \left(\frac{\sigma_o - \sigma_i}{b - a} \right)^2 + \sigma_o + (m\sigma_c\sigma_o + \sigma_c^2)^{0.5}, \quad (13)$$

where m is a material constant and varies by rock type, and μ_2 and μ_3 are the coefficients reflecting the influence of the average radial stress gradient on the σ_s .

By adopting the single and double nonlinear failure criteria, the coupled influences of the external confining stress and radial stress gradient on the triaxial compressive strength of the hollow cylindrical granite specimens can be modelled and are shown in Fig. 15b, c, respectively, based on the data listed in Table 1. For the nonlinear failure criterion models of hollow cylindrical granite specimens at $H/D = 2, 1$ and 0.5 , the regressed strength parameters, R^2 values and RMSEs are listed in Table 2.

The linear and nonlinear failure criterion models indicate that the triaxial compressive strength of a hollow cylindrical granite specimen increases with increasing external confining stress and decreasing radial stress gradient, illustrating that the external confining stress can improve the axial supporting capacity, whereas the radial stress gradient reduces this capacity. For the linear failure criterion, the values of R^2 are 0.9294, 0.9113 and 0.8932, and the RMSEs are 33.68, 34.30 and 37.67 MPa at $H/D = 2, 1$ and 0.5 , respectively. For the single nonlinear failure criterion, the values of R^2 are 0.9934, 0.9799 and 0.9698, and the RMSEs are 10.29, 16.31 and 20.04 MPa at $H/D = 2, 1$ and 0.5 , respectively. For the double nonlinear failure criterion, the values of R^2 are 0.9930, 0.9814 and 0.9702, and the RMSEs are 10.57, 15.72 and 19.92 MPa at $H/D = 2, 1$ and 0.5 , respectively. These values from the regressed models indicate that the nonlinear failure criterion is more accurate than the linear failure criterion in terms of estimating the properties of triaxial

compressive strength of hollow cylindrical granite specimens under coupled external and internal confining stresses.

5 Conclusions

Triaxial compression experiments were performed to investigate the triaxial compressive strength properties of hollow cylindrical granite specimens under a radial non-uniform confining stress field. These tests were conducted by combining the MTS-815 servo-controlled rock mechanics test system with an internal loading configuration specially designed to create a non-uniform confining stress condition with different radial stress gradients determined by the coupled external and internal confining stresses. Based on the experimental results, the following conclusions can be drawn:

1. A radial non-uniform confining stress field can be established when a hollow cylindrical granite specimen is subjected to different external and internal pressures on the outside and inside boundary faces, respectively. The average radial stress gradient is used to quantify the non-uniform contribution of the confining stress field. The triaxial compressive strength of the hollow cylindrical granite specimens present a nonlinear increase (fast followed by slow) with a decreasing average radial stress gradient at the same external confining stress and specimen L/D ratio. A moderate internal confining stress can clearly improve the triaxial bearing capacity of the hollow cylindrical granite specimens, which indicates that supporting the wall of opening is a useful measure to improve the overall compressive strength of the rock mass around the opening. The nonlinear (weak followed by strong) negative correlation between the normalized indices of the triaxial compressive strength and average radial stress gradient further confirms that a high radial stress gradient will significantly reduce the triaxial compressive strength. In addition, the external confining stress has a positive effect on the triaxial compressive strengths of the hollow cylindrical granite specimens, similar to the correlation between the conventional triaxial compressive strength of intact cylindrical specimens and the applied confining stress.
2. The evaluated external and internal confining stresses in the triaxial compression tests cannot change the failure pattern of the hollow cylindrical granite specimens. However, the failure patterns change from shear failure to coupled shear and slabbing failure and then to slabbing failure with the decrease in the specimen L/D ratios from 2 to 1 and then to 0.5; this change is due to the size and end effects. For the size effect, the short specimen can be represented as the combination of the top and

Fig. 15 Failure criteria reflecting the influences of the external confining stress and average radial stress gradient on the triaxial compressive strength of the hollow cylindrical granite specimens, according to the proposed **a** linear, **b** single non-linear and **c** double non-linear failure criterion models

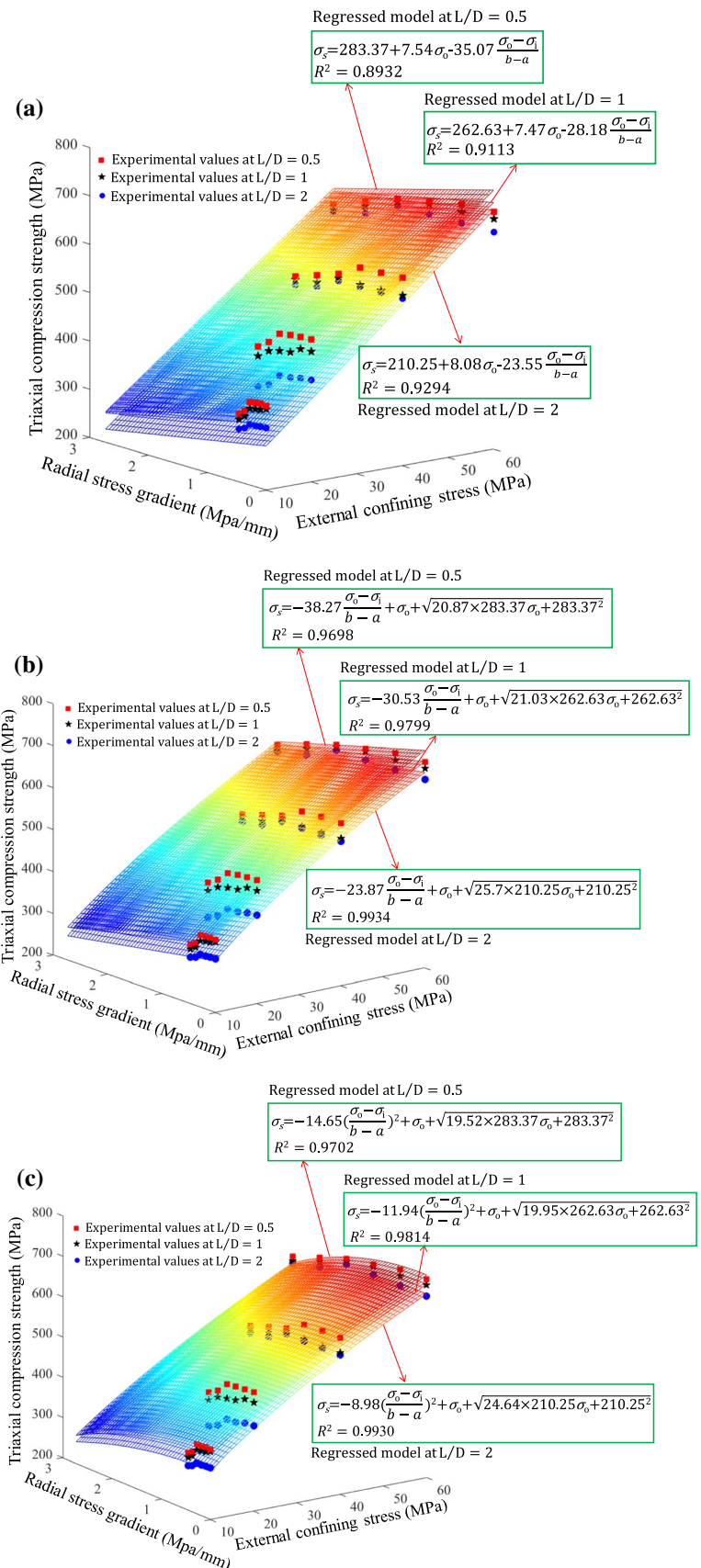


Table 2 Regressed strength parameters of the hollow cylindrical granite specimens

L/D ratio	σ_c (MPa)	Model 1 (linear criterion, Eq. 10)				Model 2 (single nonlinear criterion, Eq. 12)				Model 3 (double nonlinear criterion, Eq. 13)			
		k	μ_1	$^aR^2$	RMSE ^b (MPa)	m	μ_2	R^2	RMSE (MPa)	m	μ_2	R^2	RMSE (MPa)
2	210.25	8.08	-23.55	0.9294	33.68	25.7	-23.87	0.9934	10.29	24.64	-8.98	0.9930	10.57
1	262.63	7.47	-28.18	0.9113	34.30	21.03	-30.53	0.9799	16.31	19.95	-11.94	0.9814	15.72
0.5	283.37	7.54	-35.07	0.8932	37.67	20.87	-38.27	0.9698	20.04	19.52	-14.65	0.9702	19.92

$$^aR^2 = 1 - \frac{\sum_{i=1}^N (\sigma_{s,i}^E - \sigma_{s,i}^T)^2}{\sum_{i=1}^N (\sigma_{s,i}^E)^2}$$

^bRMSE = $\sqrt{\frac{1}{N} \sum_{i=1}^N (\sigma_{s,i}^T - \sigma_{s,i}^E)^2}$, where $\sigma_{s,i}^T$ is the theoretical value calculated by the failure criterion model, $\sigma_{s,i}^E$ is the experimental value measured in the test, and N is the number of data points

bottom quarter sections of the long specimen. For the end effect, the increase in the end effect with decreasing specimen L/D ratio will induce the rotation of the fracture at rock failure, resulting in an increase in the fracture angle, causing a variation in the failure patterns, which change from shear failure to slabbing failure.

- Due to the end effect and the change in the failure patterns, the triaxial compressive strength of a hollow cylindrical granite specimen increases with decreasing L/D ratio. The end effect, which can induce a certain lateral confinement of the specimen, can improve the measured rock strength and will increase as the L/D ratio decreases. Supported by the confining stress, the hollow cylindrical granite specimen with a low L/D ratio will undergo a plasticity stage and can sustain further loads even though many slabbing cracks may have formed.
- Based on the Mohr–Coulomb and Hoek–Brown criteria, the linear, single nonlinear and double nonlinear failure criteria were proposed to quantify the influences of the external confining stress and radial stress gradient on the triaxial compressive strength of hollow cylindrical granite specimens. The proposed failure criterion models clearly indicate that the external confining stress has a positive effect on the triaxial compressive strength of hollow cylindrical granite specimens, while the radial stress gradient presents a negative influence on their triaxial compressive strength. In addition, the goodness of fit (R^2) close to 1 and the lower root-mean-squared error (RMSE) indicate that the nonlinear failure criterion reflects the triaxial compressive strength properties more accurately than the linear failure criterion. The regressed failure criterion is based on the experimental strengths from a scaled physical simulation and is useful for tunnelling and mining engineers who perform stability analyses, referring to the rock mass around a circular opening oriented along the direction of maximum principal geostress.

Acknowledgements The work described in this paper was supported by the State Key Research Development Program of China (2016YFC0600706), the National Natural Science Foundation of China (51504287, 51774326 and 41630642) and the Hunan Provincial Natural Science Foundation of China (2017JJ3390) as well as by the China Postdoctoral Science Foundation funded project (2016M602432), for which the authors are very thankful. The corresponding author acknowledges the support of an open fund from the State Key Laboratory for Geomechanics and Deep Underground Engineering at the University of Mining and Technology-Beijing (SKLGDUEK1418).

References

- Alsayed MI (2002) Utilising the Hoek triaxial cell for multiaxial testing of hollow rock cylinders. *Int J Rock Mech Min Sci* 39(3):355–366
- Bieniawski Z, Bernede M (1979) Suggested methods for determining the uniaxial compressive strength and deformability of rock materials: Part I. Suggested method for determining deformability of rock materials in uniaxial compression. *Int J Rock Mech Min Sci Geomech Abstr* 16:138–140
- Brady BH, Brown ET (2006) *Rock mechanics: for underground mining*. Springer, Dordrecht
- Cai M, Kaiser PK (2014) In-situ rock spalling strength near excavation boundaries. *Rock Mech Rock Eng* 47(2):659–675
- Cantiemi L, Anagnostou G (2009) The effect of the stress path on squeezing behavior in tunneling. *Rock Mech Rock Eng* 42(2):289–318
- Cao W, Li X, Tao M, Zhou Z (2016) Vibrations induced by high initial stress release during underground excavations. *Tunn Undergr Space Technol* 53:78–95
- Dinis da Gama C (2012) The hollow cylinder test as an alternative to true triaxial loading of prismatic rock specimens. In: Kwasniewski M, Li X, Takahashi M (eds) *True triaxial testing of rocks*. CRC Press, Boca Raton, pp 73–82
- Drucker DC, Prager W (1952) Soil mechanics and plastic analysis or limit design. *Q Appl Math* 10(2):157–165
- Du K, Tao M, Li XB, Zhou J, (2016) Experimental study of slabbing and rockburst induced by true-triaxial unloading and local dynamic disturbance. *Rock Mech Rock Eng* 49 (9):3437–3453
- Fairhurst CE, Hudson JA (1999) Draft ISRM suggested method for the complete stress–strain curve for intact rock in uniaxial compression. *Int J Rock Mech Min Sci* 36(3):279–289

- Franklin JA (1971) Triaxial strength of rock materials. *Rock Mech* 3(2):86–98
- Han L, He Y, Zhang H (2016) Study of rock splitting failure based on griffith strength theory. *Int J Rock Mech Min Sci* 83:116–121
- Handin J, Heard HA, Magouirk JN (1967) Effects of the intermediate principal stress on the failure of limestone, dolomite, and glass at different temperatures and strain rates. *J Geophys Res* 72(2):611–640
- Heuze FE (1980) Scale effects in the determination of rock mass strength and deformability. *Rock Mech* 12(3–4):167–192
- Hoek E, Brown ET (1980) *Underground excavations in rock*. Institution of Mining and Metallurgy, London
- Hoek E, Brown ET (1997) Practical estimates of rock mass strength. *Int J Rock Mech Min Sci* 34(8):1165–1186
- Hoek E, Martin CD (2014) Fracture initiation and propagation in intact rock—a review. *J Rock Mech Geotech Eng* 6(4):287–300
- Hoskins ER (1969) The failure of thick-walled hollow cylinders of isotropic rock. *Int J Rock Mech Min Sci Geomech Abstr* 6(1):99–125
- Hua AZ, You MQ (2001) Rock failure due to energy release during unloading and application to underground rock burst control. *Tunn Undergr Space Technol* 16(3):241–246
- Jaeger JC, Cook NGW, Zimmerman RW (2007) *Fundamentals of rock mechanics*. Wiley, New York
- Lee DH, Juang CH, Chen JW, Lin HM, Shieh WH (1999) Stress paths and mechanical behavior of a sandstone in hollow cylinder tests. *Int J Rock Mech Min Sci* 36(7):857–870
- Li D, Li CC, Li X (2011) Influence of sample height-to-width ratios on failure mode for rectangular prism samples of hard rock loaded in uniaxial compression. *Rock Mech Rock Eng* 44(3):253–267
- Li X, Cao W, Zhou Z, Zou Y (2014) Influence of stress path on excavation unloading response. *Tunn Undergr Space Technol* 42:237–246
- Li X, Wang S, Wang S (2018) Experimental investigation of the influence of confining stress on hard rock fragmentation using a conical pick. *Rock Mech Rock Eng* 51(1):255–277
- Li X, Wu Q, Dong L, Chen L, Xie X, Zhang C (2015) Mechanical property of thick-walled hollow cylinders of sandstone with filling. *Chin J Geotech Eng* 37(12):2149–2156
- Martin CD, Maybee WG (2000) The strength of hard-rock pillars. *Int J Rock Mech Min Sci* 37(8):1239–1246
- Martino JB, Chandler NA (2004) Excavation-induced damage studies at the underground research laboratory. *Int J Rock Mech Min Sci* 41(8):1413–1426
- Mogi K (2007) *Experimental rock mechanics*. CRC Press, London
- Read RS (2004) 20 years of excavation response studies at AECL's Underground Research Laboratory. *Int J Rock Mech Min Sci* 41(8):1251–1275
- Sadd MH (2014) *Elasticity: theory, applications, and numerics*. Academic Press, Waltham
- Shemyakin EI, Fisenko GL, Kurlenya MV, Oparin VN, Reva VN, Glushikhin FP, Rozenbaum MA, Tropp EA, Kuznetsov YS (1986) Zonal disintegration of rocks around underground workings, part 1: data of in situ observations. *J Min Sci* 22(3):157–168
- Tao M, Li X, Wu C (2013) 3D numerical model for dynamic loading-induced multiple fracture zones around underground cavity faces. *Comput Geotech* 54:33–45
- Wiebols GA, Cook NGW (1968) An energy criterion for the strength of rock in polyaxial compression. *Int J Rock Mech Min Sci* 5(6):529–549
- Xu Y, Cai M, Zhang X, Feng XT (2017) Influence of end effect on rock strength in true triaxial compression test. *Can Geotech J* 54:862–880
- Yang SQ (2016) Experimental study on deformation, peak strength and crack damage behavior of hollow sandstone under conventional triaxial compression. *Eng Geol* 213:11–24
- Zhang H, He Y, Liu H, Han L, Shao P (2011) Ringlike failure experiment of thick-walled limestone cylinder specimens in triaxial unloading tests. *Min Sci Technol (China)* 21(3):445–450